Influence of Primary Sequence Transpositions on the Folding Pathways of Ribonuclease T1[†]

Jason L. Johnson and Frank M. Raushel*

Department of Chemistry, Texas A&M University, College Station, Texas 77843

Received December 20, 1995; Revised Manuscript Received May 31, 1996[⊗]

ABSTRACT: The slow folding of circularly permuted variants of ribonuclease T1 has been examined using steady-state and frequency−domain fluorescence spectroscopy. The sequence transpositions have previously been designed by eliminating a restrictive Cys2-Cys10 disulfide bond, adjoining the original termini with a three-peptide Gly-Gly-Gly linker, and conferring new termini to four different solvent-exposed β-turns interposing secondary structural elements [Garrett, J. B., Mullins, L. S., & Raushel, F. M. (1996) *Protein Sci. 5*, 204−211]. Each of the mutant proteins continues to be rate-limited in folding by the slow *trans* to *cis* isomerizations of Pro39 and Pro55, giving rise to a branched mechanism populated by intermediates with mixed proline isomers. However, the overall rate of folding is increased in accordance with the general destabilizing effect of each circular permutation. Steric hindrances imposed by Trp59 on the isomerization around the Tyr38-Pro39 peptide bond have been implicated in decelerating the folding of RNase T1 [Kiefhaber, T., Grunert, H.-P., Hahn, U., & Schmid, F. X. (1992) *Proteins: Struct., Funct., Genet. 12*, 171−179]; it is this tertiary restraint which appears to be variably relieved by the sequence transpositions. A fluorescence characterization of Trp59 indicates little difference between fully folded RNase T1 and the variants in terms of its lifetime, accessibility to quenchers, and rotational properties. Yet, within protein that is "completely" denatured, Trp59 exhibits variable flexibility, greatest within the circularly permuted variants folding the fastest. Such differences in the dynamic properties of Trp59 between each denatured protein may be direct evidence for a relative loosening of the tertiary fold maintaining the "deleterious" Trp59−Pro39 interaction in the partially folded intermediates.

While it is commonly recognized that the ultimate three-dimensional conformation of a protein is dictated by its amino-acid sequence, the rules governing this deterministic relationship between primary, secondary, and tertiary structure are still imprecise. Moreover, the mechanism(s) by which extended polypeptide chains bypass potentially innumerable thermodynamic "traps" to fold into a functional native state on a practical time scale remains an investigational challenge. Crucial to the understanding of the inherent selectivity of protein folding is a knowledge of the earliest nucleating interactions. To this end, circular permutations can be used to systematically assess the potential involvement of specific protein regions in direct, short-range interactions which may initiate, or at a later stage contribute to, the folding event (Goldenberg, 1989).

A circular permutation results from covalently linking the original termini and subsequently introducing amino- and carboxyl-ends in an alternate region, the net effect being a rearrangement of the primary sequence. If the transposition effectively separates either individual residues or units of secondary structure which are required to coalesce in the transition from the denatured to native state, deviations in the normal folding kinetics may be observed and potentially correlated with the perturbation. Circular permutations have been applied in limited fashion to probe mechanisms of folding for bovine pancreatic trypsin inhibitor (Goldenberg & Creighton, 1984), phosphoribosyl anthranilate isomerase (Luger *et al.*, 1989), dihydrofolate reductase (Buchwalder *et al.*, 1992), T4 lysozyme (Zhang *et al.*, 1993), aspartate transcarbamoylase (Yang & Schachman, 1993), and α-spectrin SH3 (Viguera *et al.*, 1995).

In one of the first comprehensive applications of circular permutations, Garrett *et al.* (1996) have used a novel combination of polymerase chain reaction (PCR) amplification steps (Mullins *et al.*, 1994) to introduce new termini throughout the entire polypeptide sequence of ribonuclease T1 (RNase T1),[1] a small protein composed of only 104 amino acids and stabilized by two (Cys2-Cys10 and Cys6-Cys103) disulfide bonds. The Cys2-Cys10 disulfide bond precluded the direct adjoinment of the existing termini without either introducing significant torsional strain or requiring a cumbersome linker of five or more residues. Removal of this constraint on Cys2 permitted the use of the tripeptide, Gly-Gly-Gly, to link the original termini without causing molecular strain. The disulfide bond was eliminated via substitution of both cysteines for alanines to create the C2,-10A mutant. The C2,10A variant was further modified with the linker, and new ends were separately introduced in areas of solvent-exposed loop at positions between Gly34 and Ser35 (cp35), Phe48 and Asp49 (cp49), Ser69 and Gly70 (cp70), and Ala95 and Ser96 (cp96). The locations for the

[†] Supported in part by the NIH (GM-49706) and an NRSA fellowship to J.L.J. (GM-17465).

* Author to whom correspondence may be addressed. FAX: (409) 845-9452. E-mail: raushel@tamu.edu.

[⊗] Abstract published in *Advance ACS Abstracts,* July 15, 1996.

[1] Abbreviations: RNase T1, ribonuclease T1 from *Aspergillus oryzae*; C2,10A, RNase T1 mutant with cysteines 2 and 10 replaced by alanines; cp35, cp49, cp70, and cp96, circularly permuted mutants of C2,10A with new amino-terminus positioned at Ser35, Asp49, Gly70, and Ser96, respectively, and the original termini covalently attached by a Gly-Gly-Gly linker; gdmCl, guanidinium chloride; NaOAc, sodium acetate; NATA, *N*-acetyltryptophanamide.

S0006-2960(95)03026-1 CCC: $12.00

Scheme 1

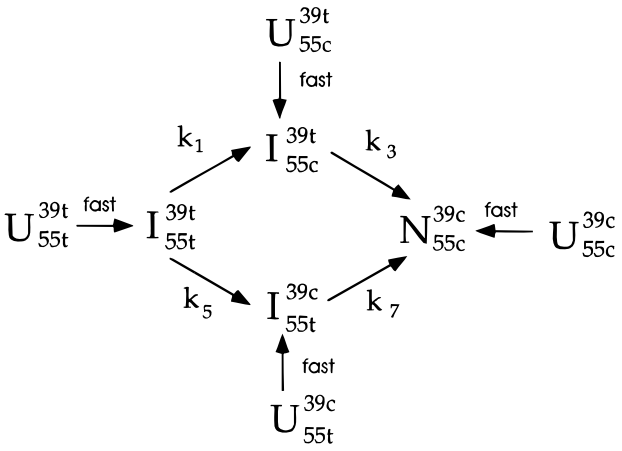

new termini were centered within each loop as far removed as possible from regions of secondary structure to avoid disruption of the β-strands and α-helix. These transpositions collectively reordered the majority of secondary structural elements in RNase T1 and disrupted four of the five β-turns (Garrett *et al*., 1996). Nevertheless, all of these mutant proteins were shown to exhibit partial ribonuclease activity (Garrett *et al.,* 1996), suggesting a final conformation for each protein analogous to that of wild-type RNase T1. To what extent each of these major alterations in primary sequence imposed deviations on the transition from the unfolded to native-like state is the subject of this investigation. Fluorescence assays (Kiefhaber *et al*., 1990b) designed to discriminate between intermediates and the more stable product of the RNase T1 folding pathway in conjunction with a time-resolved fluorescence characterization of each circularly permuted variant will highlight the impact of each transposition. Serving as a basis of comparison will be the branched folding mechanism of wild-type RNase T1 proposed by Schmid's lab (Scheme 1) (Kiefhaber *et al*., 1990a−c; Mayr *et al*., 1993; Mayr & Schmid, 1993), distinguished by rapid formation of partially folded intermediates leading into the slow, rate-limiting isomerizations of prolines 39 and 55 from the energetically favored (Grathwohl & Wuthrich, 1976) *trans* conformation in the denatured polypeptide to that of *cis*, as they are in fully folded RNase T1. In this context, cp35 and cp49 are of particular interest due to their relative proximity to Pro39 and Pro55, respectively; either of these transpositions might be likely to alter the conformational requirements of one or both prolines in the folded state.

MATERIALS AND METHODS

Materials. The pMc5TPRTQ (Steyaert *et al.*, 1990) plasmid encoding for native RNase T1 and the *Escherichia coli* strain WK6 (Zell & Fritz, 1987) were generous gifts of Professor C. N. Pace (Texas A&M University). Engineered genes for C2,10A, cp35, cp49, cp70, and cp96 in the pMc5TPRTQ plasmid are from the previous efforts of Garrett *et al.* (1996). Guanidine hydrochloride (gdmCl), ribonucleic acid core (Type IIC from *Torula* yeast), acrylamide, and potassium iodide were obtained from Sigma. All other buffers and purification reagents were of analytical grade and purchased from either Sigma, Baker, or Fisher. Deionized, distilled water was used throughout.

Growth and Purification of RNase T1. RNase T1, C2,-10A, and each of the circularly permuted variants were purified from the WK6 strain of *E. coli*, transformed with pMc5TPRTQ-derived plasmids carrying the appropriate RNase T1 gene (Garrett *et al.,* 1996) fused with a short *PhoA* leader sequence behind a *tac* promoter. The resulting overexpressed protein is directed to the periplasmic space by *PhoA* where it undergoes post-translational cleavage of the signal peptide. Transpositions of the gene sequences were accomplished via a series of three polymerase chain reactions, as described elsewhere (Garrett *et al.*, 1996). RNase T1 variants were grown and purified using a variation (Garrett *et al.,* 1996) of the method of Shirley and Laurents (1990).

Specific Activity Determination. RNase T1 activity was monitored by the continuous assay of Oshima *et al.* (1976), in which an absorbance decrease concomitant to the digestion of RNA is detected on a Gilson spectrophotometer at 298.5 nm. Protein concentrations of purified RNase T1 were determined using an extinction coefficient of 1.85×10^4 M^{-1} cm^{-1} at 278 nm (Hu *et al.*, 1992).

gdmCl-Induced Denaturation. Protein samples were incubated at 10 °C in 50 mM sodium acetate (NaOAc), pH 5.0, in the presence of various concentrations of gdmCl for 12−15 h to ensure equilibration. Fluorescence measurements were performed in a model 4800 SLM fluorimeter coupled with ISS PX01 photon counting electronics by exciting the single intrinsic tryptophan of RNase T1 (Trp59) with a 450 W xenon-arc lamp at 290 nm and monitoring its emission at 320 nm. RNase T1 concentrations were 1 μM for all steady-state measurements, and corrections were made for blank contributions. To obtain values for the stabilizing free energy of each mutant ($\Delta G_D^{H_2O}$), a two-state transition was assumed in which the resultant changes in the relative fluorescence (degree of unfolding) with increasing gdmCl concentrations were fit via a nonlinear least-squares analysis to the following equation (Santoro & Bolen, 1988):

$$y_{obs} = \frac{(y_n + m_n[D]) - (y_u + m_u[D])}{1 + \exp\{-(\Delta G_D^{H_2O} - m_G[D])/RT\}} + (y_u + m_u[D]) \quad (1)$$

where y_{obs} is the observed relative change in the total fluorescence; y_n and y_u are the percent fluorescence exhibited by native and unfolded protein, respectively, in the absence of denaturant; m_n and m_u are the slopes of the pre- and post-translational regions, respectively; R is the gas constant (1.987 cal/mol·K); T is the absolute temperature in Kelvin; m_G is the slope of the transitional region; and $\Delta G_D^{H_2O}$ is the difference in free energy between native and unfolded protein extrapolated to zero denaturant concentration.

Unfolding Kinetics. To monitor the fluorescence decrease associated with RNase T1 unfolding, each of the RNase T1 mutants was first diluted from a 25 mg/mL stock solution 20-fold into a 100 mM NaOAc solution, pH 5.0, at room temperature. In a pre-incubated cuvette at 10 °C, unfolding was initiated by a subsequent 300-fold dilution into the appropriate concentration of gdmCl, providing a final protein concentration of 0.4 μM in 1.5 mL. The fluorescence change was monitored at 320 nm following excitation at 290 nm on an SLM 8100 fluorimeter. For slower time traces extending beyond 500 s, the excitation light was interrupted by a shutter between acquisitions and the sample was continuously stirred

to alleviate potential problems associated with photobleaching.

Folding Kinetics. Initially, a 20-fold dilution of a 25 mg/mL protein stock solution into 6.3 M gdmCl and 100 mM glycine hydrochloride, pH 1.7, at 25 °C generated the denatured form of each enzyme. Within a quartz cell preincubated at 10 °C, aliquots of the unfolded protein were diluted 300-fold into 100 mM NaOAc, pH 5.0, containing variable concentrations of gdmCl. The rates of fluorescence recovery concomitant with the folding of the RNase T1 variants were monitored on the SLM 8100 with 290 nm excitation and 320 nm emission. Blank corrections were routinely performed for an accurate representation of the percentage of each phase in folding. Folding data were fit on Sigma Plot 2.0. To determine the number of exponential phases associated with each transition, increasingly more complex models were applied to the data until standard deviations were no longer improved and/or correlations between the parameters approached values of 1.

Detection of Native Molecules. Following the general scheme outlined previously (Kiefhaber *et al.*, 1990b), assays to monitor native molecule formation were performed in a series of three steps: (1) the protein was unfolded at 25 °C via a dilution to final concentrations of 6 M gdmCl and 100 mM glycine hydrochloride at pH 1.7; (2) folding was initiated at 10 °C by diluting aliquots of the unfolded sample into a sodium acetate buffer to final conditions of 0.025 M gdmCl and 100 mM NaOAc at pH 5.0; (3) at various times of folding, aliquots were removed and diluted into a cuvette at 10 °C under solution conditions in which the unfolding of all intermediates is complete within the time of mixing (<10 s), but native molecules unfold with a relaxation time of approximately 100 s. The gdmCl concentrations required to meet these criteria were empirically determined for each RNase T1 mutant. The gdmCl concentrations used in the unfolding step were 6.0 M (pH 1.8), 5.4 M (pH 2.1), 5.6 M (pH 5.0), 3.6 M (pH 5.0), 3.4 M (pH 5.0), and 5.4 M (pH 5.0) for wild-type RNase T1, C2,10A, cp35, cp49, cp70, and cp96, respectively. Final protein concentrations were 0.4 μM. Unfolding of native molecules was monitored at 320 nm after excitation at 290 nm on a model 8100 SLM fluorimeter. The amplitudes of unfolding at the various times (t) of folding relative to the amplitude of unfolding after the protein is allowed to completely fold is then proportional to the percentage of native molecules throughout the folding period.

Detection of Transient Folding Intermediates. The assay to monitor intermediate formation is generally the same protocol to detect native molecules, except that solution conditions vary in the final step. The protein was unfolded at 25 °C via dilution to final concentrations of 6 M gdmCl and 100 mM glycine hydrochloride, pH 1.7. Aliquots were removed and diluted to yield a solution of 0.025 M gdmCl and 100 mM NaOAc at pH 5.0 and 10 °C. The sample was allowed to fold under these conditions, and at various times aliquots were removed and diluted into a denaturing solution designed such that any intermediate would unfold with a relaxation time of approximately 100 s, but native molecules ideally unfold and/or fold so slowly as to not interfere with intermediate detection. These conditions must be independently established for each mutant and, when necessary, each intermediate associated with that mutant. The final protein concentration in the unfolding step of the assay was 0.4 μM, and the associated fluorescence decrease was continuously monitored at 320 nm subsequent to 290 nm excitation. The measured amplitude of unfolding was proportional to the amount of intermediate present at folding time, t.

Frequency−Domain Measurements. Frequency−domain fluorimetry was performed on an ISS K2, using the 300 nm line of a Spectra-Physics model 2045 argon ion laser as the excitation source. The excitation beam was passed through a 2 mm thick Schott WG-290 filter to remove the 275 nm line also produced by the laser in the "deep-UV" mode. Emission was collected through a 2 mm thick Schott WG-335 cut-on filter. Lifetime measurements were performed with excitation (Glan Taylor) and emission (Glan Thompson) polarizers oriented at 0° and 55°, respectively, to the vertical axis to avoid polarization artifacts (Spencer & Weber, 1970). Data analysis was performed with Globals Unlimited, obtained from the Laboratory for Fluorescence Dynamics at the University of Illinois at Urbana−Champaign. Decay models appropriate for each data set were chosen on the basis of minimizing values of κ^2 as described previously (Jameson *et al.*, 1984), using expected standard deviations of 0.2 and 0.004 for phase and modulation, respectively. Protein concentrations for lifetime and dynamic anisotropy measurements on the folded state were 40 μM in 100 mM NaOAc, pH 5.0, at 10 °C. The unfolded form of each protein was generated by preincubation for at least 12 h in 6 M gdmCl and 100 mM NaOAc, pH 5.0, at 10 °C. Frequency−domain measurements were taken at 10 °C with final unfolded protein concentrations of 100 μM.

Iodide and Acrylamide Quenching. Lifetime measurements of the single intrinsic tryptophan of each RNase T1 mutant in the folded state were made at iodide ion or acrylamide concentrations of 0, 0.1, 0.2, 0.3, 0.4, and 0.5 M. Determinations of fluorescence lifetimes for each unfolded protein were performed at 0, 0.05, 0.10, 0.15, 0.20, and 0.25 M quencher concentration. Each group of six data sets was globally linked in terms of the percent of each species in solution and fit on the Globals Unlimited program to the following equation:

$$\frac{\tau^0}{\tau} = 1 + \tau^0 k_{SV}[Q] \qquad (2)$$

where τ^0 is the lifetime in the absence of quencher Q, τ is the apparent lifetime at a particular quencher concentration, and k_{SV} is the Stern-Volmer bimolecular collisional rate constant between Q and the excited state of tryptophan.

RESULTS

gdmCl-Induced Unfolding Transitions. Denaturation profiles (Figure 1) were fit to eq 1 using a nonlinear least-squares analysis to obtain values for m_G and $\Delta G_D^{H_2O}$, shown in Table 1. While the m_G values are essentially identical between native RNase T1 and the mutant lacking the Cys2-Cys10 disulfide bond, the circularly permuted variants (cp49 and cp70, in particular) have slightly elevated values for m_G, suggesting a greater difference in interaction of the denaturant with the native and denatured states, respectively (Tanford, 1968; Schellman, 1978; Pace, 1986). The relative values for $\Delta G_D^{H_2O}$ follow the same trends as those previously published for urea-induced unfolding at 25 °C (Garrett *et al.*, 1996). The midpoint of unfolding, $[gdmCl]_{0.5}$, for each

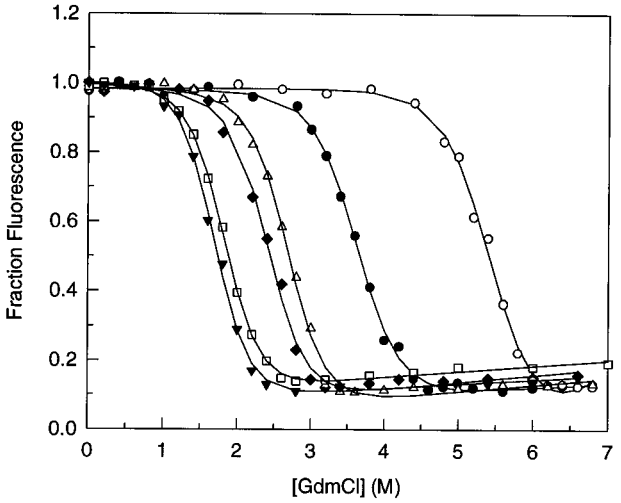

FIGURE 1: gdmCl-induced unfolding transitions at 10 °C, pH 5.0, of wild-type RNase T1 (○), C2,10A (●), cp35 (△), cp49 (▼), cp70 (□), and cp96 (◆). Fluorescence emission was monitored at 320 nm following excitation at 290 nm, and data were fit to eq 1 to provide values for $[gdmCl]_{1/2}$, m_G, and $\Delta G_D^{H_2O}$ (see Table 1).

Table 1: Stabilities from Denaturation Profiles at 10 °C, pH 5.0

protein	$[gdmCl]_{1/2}$ (M)	m_G (kcal/mol·M)	$\Delta G_D^{H_2O}$ (kcal/mol)
wt	5.18 ± 0.63	−1.84 ± 0.16	9.54 ± 0.81
C2,10A	3.61 ± 0.33	−1.87 ± 0.12	6.75 ± 0.45
cp35	2.69 ± 0.32	−2.18 ± 0.18	5.87 ± 0.50
cp49	1.69 ± 0.18	−2.35 ± 0.16	3.98 ± 0.31
cp70	1.83 ± 0.11	−2.30 ± 0.90	4.20 ± 0.18
cp96	2.42 ± 0.37	−2.15 ± 0.23	5.21 ± 0.59

curve can be estimated according to the following equation (Santoro & Bolen, 1988):

$$[gdmCl]_{0.5} = \frac{-\Delta G_D^{H_2O}}{m_G} \quad (3)$$

Values for $[gdmCl]_{0.5}$ are reported in Table 1.

Unfolding Kinetics. The unfolding of each variant at pH 5.0 was monitored via a ∼10-fold decrease in fluorescence intensity at 320 nm and 10 °C. The gdmCl concentration was varied for each protein through a range ensuring complete unfolding and providing relaxation times between 10 and 5000 s. In every case, unfolding could be modeled as a single exponential decay consistent with a two-state transition. Accordingly, the following equation was used to relate the rate of unfolding (k_u) to denaturant concentration (Tanford, 1968; Pace, 1986):

$$\ln k_u = \ln k_u^{H_2O} + m_{ku}[gdmCl] \quad (4)$$

where $k_u^{H_2O}$ is the unfolding rate constant in water and m_{ku} is the slope of denaturation. Plots of ln k_u vs [gdmCl] (Figure 2) were sufficiently linear in each case to estimate an unfolding rate constant extrapolated to zero denaturant concentration. Calculated unfolding rate constants in acetate buffer at 10 °C are approximately 8×10^{-11}, 8×10^{-10}, 3×10^{-9}, 5×10^{-9}, 2×10^{-6}, and 1×10^{-6} s^{-1} for wild-type RNase T1, C2,10A, cp35, cp96, cp70, and cp49, respectively.

Folding Kinetics. In contrast to the unfolding kinetics, folding in the presence of 0.05 M gdmCl was more complex in each case, best described by a "fast" phase complete in the time of mixing (10 s) followed by a two-exponential rise

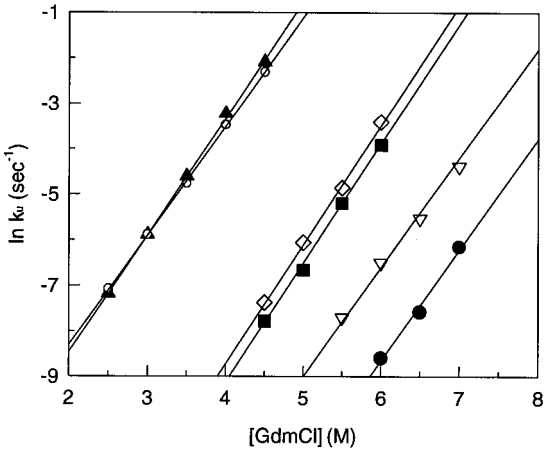

FIGURE 2: Variation of rate constants for unfolding with gdmCl concentration at 10 °C, pH 5.0, for wild-type RNase T1 (●), C2,-10A (▽), cp35 (■), cp49 (○), cp70 (▲), and cp96 (◇). The lines drawn represent the best linear fit to eq 4.

in fluorescence. Using the terminology of Schmid (Kiefhaber *et al.*, 1990a,b), the biphasic transition is comprised of an "intermediate" phase with a relaxation time (τ) of 300−500 s and a "very slow" phase with $\tau = 1300-5000$ s. Table 2 lists the particular rate constant for each phase of each RNase T1 variant as well as the percentages of the total fluorescence change attributed to each phase. While the "fast" phase accounts for approximately 38% of the fluorescence increase in wild-type RNase T1, its contribution substantially drops to less than 21% in C2,10A and the circularly permuted variants. This loss of the "fast" phase in the mutants almost equally coincides with a gain in the "intermediate" population in all but cp49, in which the pre-exponential amplitude of the "very slow" phase predominates. Accordingly, the percentage of molecules in the "very slow"phase shows little variation between the remaining five RNase T1 proteins.

Folding buffers were also adjusted to contain final gdmCl concentrations of 0.4, 0.8, and 1.5 M. The fluorescence recovery under these solution conditions again is best described by the sum of three separate phases (Table 2). However, as noted previously (Kiefhaber *et al.*, 1990b), increasingly destabilizing conditions lead to a predictable decrease in the recovery rate of the "intermediate" phase at 0.8 M gdmCl, but a somewhat surprising *increase* in the folding rate of the "very slow" phase. Elevated folding rates are noted for C2,10A, cp35, and cp96 as well when gdmCl concentrations are increased. In addition, a systematic decrease in the proportion of the "fast" phase occurs in every case as solution conditions become more denaturing.

Detection of Native Molecules. During folding, the formation of native RNase T1 molecules, as opposed to intermediates with native-like fluorescence properties, were directly followed using assays previously established in Schmid's lab (Kiefhaber *et al.*, 1990b). In almost all cases, the kinetics of native molecule formation (Figure 3) are best described as the sum of two exponentials, with a fast phase complete in the dead-time of the experiment (10 s) contributing to 3%−4% of the population. The exception lies with cp49, for which a monophasic exponential rise satisfactorily describes the slow fluorescence recovery following the rapid 3% increase. The total folding process is complete in a shorter period of time for the circularly permuted variants than for C2,10A and, to a greater extent, than for wild-type

Table 2: Kinetics of Fluorescence Recovery during Refolding at 10 °C, pH 5.0[a]

[gdmCl][b]		wt	C2,10A	cp35	cp49	cp70	cp96
0.05 M	k_1	3.2×10^{-3}	2.3×10^{-3}	3.4×10^{-3}	6.0×10^{-3}	2.2×10^{-3}	2.4×10^{-3}
	k_2	2.0×10^{-4}	2.5×10^{-4}	2.8×10^{-4}	8.0×10^{-4}	2.6×10^{-4}	4.8×10^{-4}
	$A_{\text{very slow}}$	41	37	49	69	43	42
	$A_{\text{intermediate}}$	20	42	28	16	43	36
	A_{fast}	38	21	23	15	14	23
0.4 M	k_1	3.3×10^{-3}	2.4×10^{-3}	2.5×10^{-3}	1.0×10^{-2}	2.5×10^{-3}	3.7×10^{-3}
	k_2	2.0×10^{-4}	2.9×10^{-4}	4.1×10^{-4}	7.4×10^{-4}	2.7×10^{-4}	5.3×10^{-4}
	$A_{\text{very slow}}$	49	40	44	80	79	69
	$A_{\text{intermediate}}$	21	41	35	6	18	27
	A_{fast}	30	19	21	14	3	4
0.8 M	k_1	1.9×10^{-3}	2.5×10^{-3}	2.8×10^{-3}	c	2.4×10^{-3}	3.6×10^{-3}
	k_2	1.9×10^{-4}	4.3×10^{-4}	4.0×10^{-4}	6.6×10^{-4}	2.0×10^{-4}	3.3×10^{-4}
	$A_{\text{very slow}}$	42	52	65	88	93	87
	$A_{\text{intermediate}}$	37	37	34		6	10
	A_{fast}	21	11	1	12	1	3
1.5 M	k_1	9.9×10^{-3}	4.0×10^{-3}	8.1×10^{-3}	n/a[d]	n/a	n/a
	k_2	9.3×10^{-4}	2.7×10^{-4}	1.8×10^{-4}	n/a	n/a	n/a
	$A_{\text{very slow}}$	69	87	93	n/a	n/a	n/a
	$A_{\text{intermediate}}$	11	8	4	n/a	n/a	n/a
	A_{fast}	20	5	3	n/a	n/a	n/a

[a] All kinetic parameters were obtained within a relative error of ±7%. The rate constants k_1 and k_2 refer to rate constants (in s^{-1}) for the "intermediate" and "very slow" phases of fluorescence recovery, respectively, and *A* refers to the fractional contribution (in %) of the total refolding amplitude of the corresponding phase. [b] Refers to final concentration of guanidine hydrochloride in refolding step. [c] These data fit best to a single exponential decay, corresponding closest to the "very slow" phase. [d] The proteins cp49, cp70, and cp96 are not stable at a gdmCl concentration of 1.5 M.

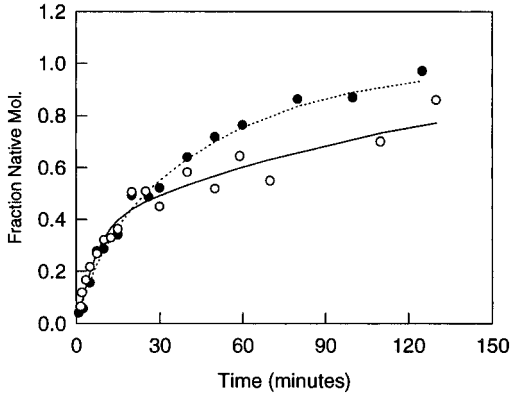

FIGURE 3: Kinetics of native molecule formation for wild-type RNase T1 (○, —) and cp35 (●, - - -) at 10 °C, pH 5.0. The lines drawn represent the best nonlinear regression fit of the data to eq 6. The fractions of native molecules at each folding time are calculated from the ratio of the unfolding amplitude at time *t* to the amplitude at $t = \infty$ (~4 h). The rate constants k_5 and k_7 deriving from each fit are provided in Table 3.

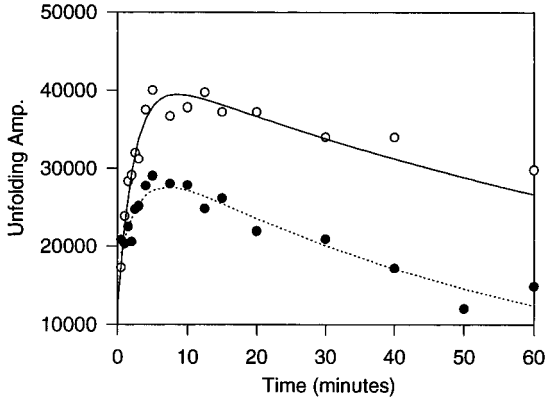

FIGURE 4: Transient formation of intermediates in the course of folding at 10 °C, pH 5.0 for wild-type RNase T1 (○, —) and cp35 (●, - - -). The unfolding amplitudes, *i.e.*, the amplitudes of the single-exponential fit of each unfolding transition, in these assays are proportional to intermediate concentration and are plotted vs the time of folding. Lines drawn are the best fit of eq 5 to the data. The rate constants k_1 and k_3 from each fit are given in Table 3.

RNase T1. Additional information is required before the kinetics of native RNase T1 formation, as it pertains to Scheme 1, can be fully interpreted. The independent quantitation of transient intermediate accumulation and decline can help, in this regard, to reduce the number of unknown parameters prior to evaluating native molecule formation within the context of the branched folding mechanism of Scheme 1.

Transient Intermediate Detection. For each of the six proteins, as least one intermediate was detected. For cp96, two distinct species were present; however, the kinetics of the least stable form could not be quantified because of the complexities associated with differentiating it from the more stable intermediate as well as the background formation of native molecules in the final unfolding step of the assay. Therefore, the denaturant concentration in the unfolding step was adjusted to follow solely the kinetics of the more stable intermediate, in which its less stable counterpart could not survive the mixing time. Additional complexities accompanied the fluorescence changes of the final assay step of cp49 and cp70; each had to be fit to a model of a single exponential decay associated with intermediate unfolding plus a linear increase or decrease associated with the early stages of native molecule folding or unfolding. To attain relaxation times in the range of 50−100 s for the unfolding step of the respective intermediates, gdmCl concentrations of 3.30, 2.56, 2.00, 1.90, 1.72, and 2.20 M at pH 5.0 were used for wild-type RNase T1, C2,10A, cp35, cp49, cp70, and cp96, respectively. Plots of the unfolding amplitude vs folding times are shown for wild-type RNase T1 and cp35 in Figure 4. Partially folded intermediates are formed for each mutant in at least two steps; an initial reaction generates transient molecules rapidly in the time of mixing, while a second reaction slowly forms the intermediate with a relaxation time ranging from 50 to 200 s. A much slower reaction then depletes the intermediate pool.

Scheme 2

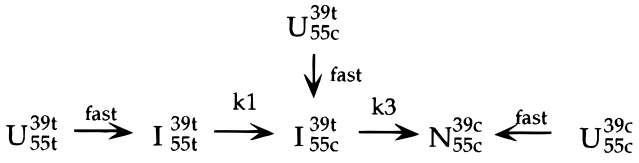

Kinetic Analyses of Intermediate and Native Molecule Formation. As shown in Scheme 1, the RNase T1 folding mechanism was developed in Schmid's lab (Kiefhaber *et al.*, 1990b,c; Mayr *et al.*, 1993; Mayr & Schmid, 1993) around the slow isomerizations of prolines 39 and 55. Native RNase T1 is depicted as N_{55c}^{39c}, where the superscript and subscript refer to prolines 39 and 55 in the *cis* (c) conformation. When the protein is denatured, the majority of unfolded molecules assume energetically favorable peptide *trans* bonds around both prolines, designated as U_{55t}^{39t}. There also exist smaller populations of unfolded protein forms having combinations of proline isomers: U_{55c}^{39t}, in which proline 39 is *trans* and proline 55 is *cis*; U_{55t}^{39c}, in which proline 39 is *cis* while proline 55 is *trans*; and U_{55c}^{39c}, in which both prolines are *cis*. Three of these unfolded species rapidly form secondary structure and enter the folding mechanism at separate points as intermediates (I) and subsequently progress through the slow rate-limiting isomerization reactions to N_{55c}^{39c}. The remaining species, U_{55c}^{39c}, can directly fold in a very fast step to native molecule N_{55c}^{39c}.

In a series of mutational studies (Kiefhaber *et al*., 1990c, 1992; Mayr & Schmid, 1993), proline 39 was identified as exhibiting the slowest isomerization rate by an order of magnitude during the $I_{35c}^{39t} \rightleftharpoons N_{55c}^{39c}$ transition. Kiefhaber *et al*. (1990b) also demonstrated that 72% of the folding molecules progress through the upper branch of the pathway involving this "very slow" step. Therefore, at least for wild-type RNase T1, I_{55c}^{39t} represents the predominant intermediate detected in the unfolding assays described above. This being the case, the branched mechanism of Scheme 1 can be simplified to the following to describe the kinetic accumulation and decay of detectable transient folding intermediates in Figure 4 (see Scheme 2). The equation derived for Scheme 2 is given as

$$[I_{55c}^{39t}] = \left\{\left(\frac{k_1(A)}{(k_3 - k_1)}\right)(e^{-k_1 t} - e^{-k_3 t}) + C(e^{-k_3 t})\right\} \quad (5)$$

where k_1 and k_3 represent the corresponding rate constants in Scheme 2, A is the amplitude of intermediate accumulation, and C is the contribution to the total amplitude from the very fast reaction $U_{55c}^{39t} \rightarrow I_{55c}^{39t}$ and/or $U_{55t}^{39t} \rightarrow I_{55t}^{39t}$ step(s). Data as in Figure 4 were fit to eq 5 to determine values for k_1 and k_3 for the RNase T1 variants.[2] The rate constants are reported in Table 3 along with values for the total amplitude, A, and contributing "fast-phase" amplitude, C. The rate constants obtained from the fit of the data to the more stable intermediate of cp96 were designated as k_5 and k_7. Two distinct folding intermediates had been identified for the variant cp96, as opposed to only one for the remaining proteins. Only the most stable of the transients (I_{55t}^{39c}) could unambiguously be followed, and the rate constants describing its progression, as noted below, corresponded more with the values for k_5 and k_7 of the other five proteins.

Table 3: Refolding Rate Constants (in min^{-1}) for RNase T1 Variants at 10 °C, pH 5.0[a]

	k_1	k_3	k_5	k_7
wt	0.44 ± 0.09 (140 s)	0.008 ± 0.001 (7500 s)	0.23 ± 0.03 (260 s)	0.18 ± 0.05 (340 s)
C2,10A	0.47 ± 0.09 (130 s)	0.009 ± 0.002 (6300 s)	0.40 ± 0.05 (150 s)	0.06 ± 0.01 (1200 s)
cp35	0.34 ± 0.11 (180 s)	0.016 ± 0.002 (3800 s)	0.19 ± 0.04 (320 s)	0.09 ± 0.03 (700 s)
cp49	0.50 ± 0.17 (120 s)	0.027 ± 0.002 (2200 s)	0.80 ± 0.17 (80 s)	0.04 ± 0.01 (1400 s)
cp70	0.79 ± 0.60 (80 s)	0.021 ± 0.006 (2800 s)	0.34 ± 0.09 (180 s)	0.10 ± 0.03 (610 s)
cp96	0.31 ± 0.11 (200 s)	0.012 ± 0.003 (5400 s)	0.46 ± 0.10 (130 s)	0.05 ± 0.01 (1300 s)

[a] Rate constants refer to those in Scheme 1. Numbers given in parentheses represent the corresponding relaxation times. Values for the amplitude (A) of intermediate accumulation obtained from a fit of eq 8 to the data in Figure 4 are $(3.0 \times 10^4 \pm 3 \times 10^3)$, $(1.5 \times 10^4 \pm 2 \times 10^3)$, $(1.5 \times 10^4 \pm 2 \times 10^3)$, $91.3 \times 10^4 \pm 2 \times 10^3)$, $(2.7 \times 10^3 \pm 1 \times 10^3)$, and $(1.5 \times 10^4 \pm 2 \times 10^3)$ for each protein as listed. Corresponding values of C, the contribution to the amplitude of intermediate accumulation deriving from the "fast" phase, are $(1.2 \times 10^4 \pm 3 \times 10^3)$, $(6 \times 10^3 \pm 2 \times 10^3)$, $(1.7 \times 10^4 \pm 2 \times 10^3)$, $(1.7 \times 10^4 \pm 2 \times 10^3)$, $(1.7 \times 10^3 \pm 1.2 \times 10^3)$, and $(1.5 \times 10^4 \pm 1 \times 10^3)$.

Assuming that the majority of molecules enter the folding pathway through the $U_{55t}^{39t} \rightarrow I_{55t}^{39t}$ step (Kiefhaber *et al.*, 1990b), the following equation can be derived for the isomerization reactions in the branched folding mechanism of Scheme 1:

$$[N_{55c}^{39c}] = 0.97\left\{1 - (e^{-(k_1+k_5)t}) - \left(\left(\frac{k_1}{(k_3 - (k_1 + k_5))}\right)(e^{-(k_1+k_5)t} - e^{-k_3 t})\right) - \left(\left(\frac{k_5}{(k_7 - (k_1 + k_5))}\right)(e^{-(k_1+k_5)t} - e^{-k_7 t})\right)\right\} + 0.03 \quad (6)$$

where k_1, k_3, k_5, and k_7 are the corresponding rate constants of Scheme 1, "0.03" represents the fraction of native molecules formed in the very fast step of $U_{55c}^{39c} \rightarrow N_{55c}^{39c}$, and "0.97" accounts for the remaining fraction of native molecules in the folding process. An unconditional fit of the data in Figure 3 to eq 6 yields values for the four rate constants with unacceptably large absolute errors. However, by fixing k_1 and k_3 (or k_5 and k_7, for cp96) in eq 6 to those values determined independently from kinetic analyses of intermediate formation, it is then possible to determine k_5 and k_7 (or k_1 and k_3, for cp96) unambiguously. Values for k_5 and k_7 resulting from this strategy are reported in Table 3.

Tryptophan Lifetime of RNase T1 Variants. The frequency dependence of phase and modulation of the single intrinsic

[2] The specific reaction scheme for wild-type RNase T1 folding has been verified via substitutional mutations of Pro39 and Pro55 (Kiefhaber *et al.*, 1990c; Mayr & Schmid, 1993). Although there is no comparable direct evidence that Scheme 1 also describes the folding kinetics of the cp mutants, the high phenomenological similarity in the nature of fluorescence recovery, native molecule formation, and intermediate accumulation between wild-type RNase T1 and the transposed mutants warrant interpretation within the same context. Rate constants for the slowest decaying intermediate are therefore by analogy assigned to be k_1 and k_3 in each case.

Table 4: Trp59 Characteristics in Circularly Permuted Variants of RNase T1 at 10 °C, pH 5.0[a]

	lifetime[b]		rotation[c]			accessibility, k_{SV} ($M \cdot ns^{-1}$)	
protein	$\tau 1$ (ns)	$f1$ (%)	Pol	r_0	$\phi 1$ (ns)	acrylamide[d]	iodide[e]
wt	4.17 ± 0.02	99.5 ± 0.1	0.300 ± 0.001	0.33 ± 0.01	8.43 ± 0.19	0.100 ± 0.004	0.013 ± 0.004
C2,10A	4.14 ± 0.04	99.2 ± 0.2	0.298 ± 0.002	0.33 ± 0.01	7.95 ± 0.18	0.090 ± 0.004	0.012 ± 0.003
cp35	4.13 ± 0.03	99.3 ± 0.2	0.301 ± 0.001	0.33 ± 0.01	8.94 ± 0.18	0.098 ± 0.005	0.015 ± 0.004
cp49	4.03 ± 0.03	99.4 ± 0.1	0.300 ± 0.001	0.33 ± 0.01	8.75 ± 0.16	0.107 ± 0.006	0.018 ± 0.004
cp70	3.79 ± 0.03	99.4 ± 0.2	0.302 ± 0.001	0.33 ± 0.01	8.55 ± 0.23	0.070 ± 0.005	0.015 ± 0.004
cp96	4.19 ± 0.04	99.7 ± 0.2	0.300 ± 0.001	0.33 ± 0.01	8.60 ± 0.20	0.096 ± 0.003	0.018 ± 0.003

[a] Symbols used in this table correspond to the following parameters: $\tau 1$, fluorescence lifetime of major component; $f1$, fractional intensity of major lifetime component; pol, steady-state polarization; r_0, limiting anisotropy; $\phi 1$, rotational correlation time; k_{SV}, bimolecular collisional rate constant. [b] Data were fit to a model allowing for two discrete exponentials, with less than 1% assigned to a scatter component. κ^2 values of 0.86, 3.40,1.24, 0.89, 2.16, and 2.63 were obtained for each fit, respectively. [c] Data fit best to a single-rotator model, corresponding to the rotation of the macromolecule. Corresponding κ^2 values are 1.90, 1.91, 1.24, 1.14, 2.25, and 1.82, respectively. [d] Global κ^2 values for six data sets ranging from 0 to 0.5 M acrylamide were deterimined as 1.15, 1.67, 2.20, 2.90, 1.85, and 1.08, respectively. The k_{SV} for NATA under comparable conditions is 4.17 ± 0.09. [e] Global κ^2 values for six data sets ranging from 0 to 0.5 M KI were determined as 1.98, 1.22, 2.02, 1.65, 1.80, and 1.01, respectively. The k_{SV} for NATA under comparable conditions is 3.20 ± 0.07.

Table 5: Trp59 Characteristics in Circularly Permuted Variants of RNase T1 Denatured in 6 M gdmCl at 10 °C, pH 5.0[a]

	lifetime[b]			accessibility, k_{SV} ($M \cdot ns^{-1}$)			
				acrylamide[c]		iodide[d]	
protein	$\tau 1$ (ns)	f1 (mol %)	$\tau 2$ (ns)	for $\tau 1$	for $\tau 2$	for $\tau 1$	for $\tau 2$
wt	4.46 ± 0.03	60.7 ± 0.4	1.29 ± 0.02	0.972 ± 0.021	3.04 ± 0.16	0.733 ± 0.025	1.35 ± 0.34
C2,10A	4.49 ± 0.05	58.0 ± 0.6	1.38 ± 0.04	0.971 ± 0.010	2.82 ± 0.15	0.671 ± 0.012	2.07 ± 0.15
cp35	4.45 ± 0.08	54.7 ± 1.0	1.54 ± 0.05	1.17 ± 0.030	3.01 ± 0.34	0.716 ± 0.024	2.66 ± 0.28
cp49	4.24 ± 0.10	59.0 ± 1.6	1.72 ± 0.08	1.25 ± 0.03	3.51 ± 0.27	0.783 ± 0.023	2.93 ± 0.29
cp70	4.50 ± 0.12	50.0 ± 2.1	1.66 ± 0.08	1.03 ± 0.03	3.23 ± 0.18	0.721 ± 0.030	2.37 ± 0.25
cp96	4.53 ± 0.09	56.4 ± 1.4	1.83 ± 0.7	1.13 ± 0.02	3.42 ± 0.02	0.697 ± 0.020	2.72 ± 0.23

[a] Symbols used in this table correspond to the following: $\tau 1$, fluorescence lifetime of first component; $f1$, mole percentage of long-lifetime component; $\tau 2$, fluorescence lifetime of second component; k_{SV}, bimolecular collisional rate constant. [b] Data were fit to a model allowing for two discreet exponential lifetimes. Values for κ^2 are 0.80, 2.34, 5.22, 7.53, 3.05, and 5.70, respectively. [c] Global κ^2 values for the six data sets ranging from 0 to 0.25 M acrylamide are 2.14, 2.31, 2.96, 3.24, 3.14, and 1.20. [d] Global κ^2 values for the six data sets ranging from 0 to 0.25 M KI are 4.60, 1.23, 3.92, 3.37, 5.58, and 2.92.

tryptophan (Trp59) was monitored for fully folded wild-type RNase T1, C2,10A, and each of the four circularly permuted variants at 10 °C, pH 5.0. In every case, over 99% of the fluorescence emission could be attributed to a single discrete exponential decay. The remaining very small fraction corresponded to a lifetime of 0 ns, representing traces of Raman scatter through the WG-335 Schott filter. The lifetimes (τ) of the tryptophan component for each enzyme are shown in Table 4. Values for τ are nearly identical in each case (~4.1 ns), although cp70 demonstrated a slightly reduced fluorescence decay time (~3.8 ns). The value of 4.17 ns for wild-type RNase T1 is consistent with other values reported at pH 5.0 (Eftink, 1983; Lakowicz *et al.*, 1983; James *et al.*, 1985; Eftink & Ghiron, 1987).

When the RNase T1 proteins are equilibrated under denaturing conditions of 6 M gdmCl, pH 5.0, the decay of tryptophan fluorescence in the RNase T1 proteins can no longer be described by a simple single exponential but is better fit by a model allowing for two discrete exponential decays (Table 5). The longer lifetime component ($\tau 1$) represents on a mole percentage basis approximately 50%−60% of the populated species and is between 4.2 and 4.6 ns. The remaining 40%−50% is best described by a lifetime ($\tau 2$) of only 1.3−1.8 ns. Values for $\tau 2$ are slightly less for the more stable wild-type and C2,10A proteins (1.3−1.4 ns) than for the circularly permuted variants (1.5−1.8 ns). Attempts to apply a distributional analysis to the fluorescence decay of Trp59 in each protein resulted in κ^2 values approximately 10-fold greater than those from the two-exponential fit. This discrete nature of the fluorescence decay even under non-native conditions has also been reported by Gryczynski *et al.* (1988).

Rotational Characteristics of the Intrinsic Tryptophan in RNase T1 Variants. Steady-state polarization measurements of Trp59 gave a value of ~0.30 for each of the proteins at 10 °C, pH 5.0, indicating little to no difference in the *average* rotational characteristics between the six proteins. To assess potential differences which may exist between the discrete modes of rotation, i.e., global vs local rotation, available to the indole moiety in each of the proteins, differential polarized phase/modulation fluorimetry was employed. The frequency spectra of the differential phase and modulation are shown in Figure 5 for native RNase T1. The data in every case fit best to a model allowing for only a single exponential anisotropy decay:

$$r(t) = r_0 e^{-t/\phi} \tag{7}$$

where r_0 is the anisotropy when $t = 0$ and ϕ is the correlation time for the diffusion process. The value of r_0 was independently found to be 0.33 ± 0.01 in all cases. The measured rotational correlation time (ϕ) for this decay was between 8 and 9 ns (Table 4), a time period slightly higher than would be expected for the global rotation at 10 °C of a fully hydrated RNase T1 molecule (Perrin, 1926; Weber, 1952) but consistent with previous reports (James *et al.*, 1985; Chen *et al.*, 1987). When the differential anisotropy data were modeled by a more complex two-exponential decay, the second rotational component was assigned by the best fit of Globals Unlimited a fractional contribution of 0%.

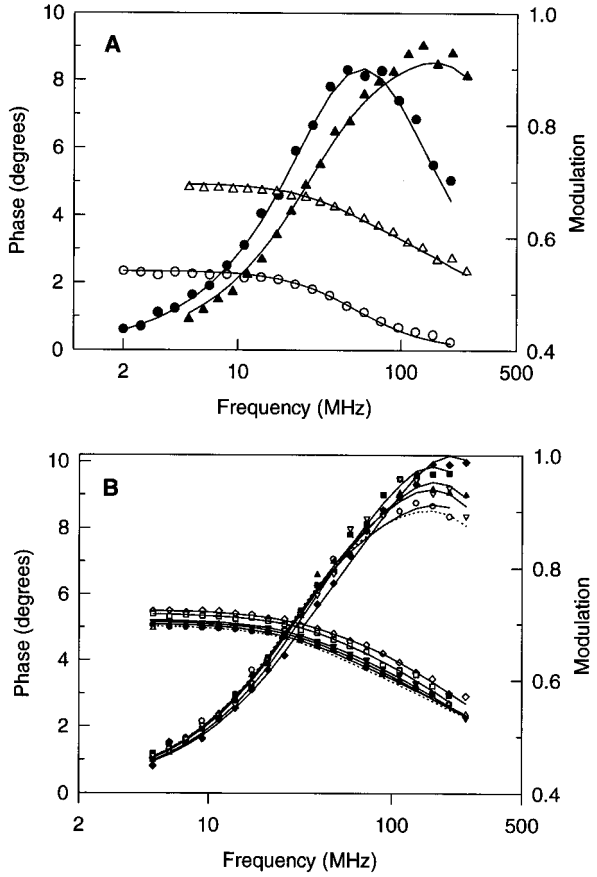

FIGURE 5: Dynamic anisotropy frequency spectra for RNase T1 variants at 10 °C, pH 5.0. (A) The variations of phase and modulation differences with frequency are shown for fully folded RNase T1 (● and ○, respectively) and for RNase T1 denatured in 6 M gdmCl (▲ and △, respectively). The lines drawn represent the best fit to a model allowing for a single rotational anisotropy decay (folded RNase T1) or for a non-associative two-exponential decay (unfolded RNase T1). (B) A comparison is shown between the frequency spectra of each RNase T1 variant unfolded in 6 M gdmCl. Phase and modulation differences are represented for C2,10A (○,●), cp35 (▲,△), cp49 (■,□), cp70 (◆,◇), and cp96 (▽,▼), and a dashed line is used to reference wild-type RNase T1. All solid lines represent the best fit of each data set to a hindered local motion plus global protein motion model. Values for corresponding rotational parameters are shown in Tables 4 and 6. Note that differences in phase between the proteins predominate at the higher frequencies which preferentially weight the fast, local rotations of Trp59.

These data therefore suggest that the indole moiety within RNase T1 and its circularly permuted variants is immobile, having little to no contribution by local motion to the depolarization mechanism.

When the proteins were denatured in 6 M gdmCl, the dynamic anisotropy frequency spectrum required a more complex model to describe the data for each of the six proteins (Figure 5B). No longer did a single exponential anisotropy decay fit the data. Instead, the phase and modulation changes in Figure 5B fit best in each case to a double exponential or, more specifically, a hindered local motion plus global protein rotation model (Munro *et al.*, 1979; Lipari & Szabo, 1980)

$$r(t) = (r_0 - r_\infty)e^{-t/\phi 1} + r_\infty e^{-\tau/\phi 2} \qquad (8)$$

where r_0 is the anisotropy in the absence of rotational diffusion (at $t = 0$), r_∞ is the anisotropy approached as a result of the depolarizing effects of the hindered rotation, and $\phi 1$ and $\phi 2$ are rotational correlation times associated with the two modes of rotation such that $\phi 1 \ll \phi 2$. Moreover, for a given protein, each of the lifetime components ($\tau 1$ and $\tau 2$) present at 6 M gdmCl can be described by distinctly different sets of rotational parameters, i.e., a non-associative fit of both lifetimes to a *single* local motion and a *single* global rotation appears inadequate. In order to discriminate between the two sets of rotational parameters, the subscript "-l" or "-s" is appended to each variable symbol to identify the long- or short-lifetime species, respectively.

Because $\phi 2_{-l}$ and $\phi 2_{-s}$ were invariant between the six unfolded proteins in independent analyses, the dynamic anisotropy data were globally analyzed with these rotational times linked across all data sets and to each other. The limiting anisotropy r_0, theoretically independent of the rotational mechanism, was also linked between the data sets. Lifetimes were fixed to those values in Table 5. Results of this fit for the rotational parameters under denaturing conditions are shown in Table 6 for wild-type RNase T1, C2,10A, and each of the circularly permuted variants. Most notably, the rotational correlation times for the tryptophan in its microenvironment, regardless of the particular RNase T1 mutant, are approximately 10-fold greater for the longer lifetime species than the component with the shorter fluorescence lifetime.

In order to make a more direct comparison of the Trp59 properties between the proteins themselves, the simpler model in which a single set of rotational parameters was assigned to both lifetimes simultaneously was also applied to the data of Figure 5b. The results are listed in Table 6. Although the global κ^2 value is slightly elevated by this simplification (from 1.08 to 1.39), the reduction in the number of variables significantly decreases associated errors. The rate of local motion, $\phi 1$, shows little variation in this approach between the mutants, although its value for cp70 is slightly lowered relative to the other five proteins. Differences are more obvious and systematic in the pre-exponential factor; all of the transposed mutants have higher values for "$r_0 - r_\infty$", with that of cp49 and cp79 elevated the most. It is possible to model these hindered fast rotation differences as rotations within a cone (Munro *et al.*, 1979; Lipari & Szabo, 1980; Gratton *et al.*, 1986; Johnson & Reinhart, 1994):

$$\Phi = \cos^{-1}\left(\frac{1}{2}\left\{\left[1 + 8\left(\frac{r_\infty}{r_0}\right)^{1/2}\right]^{1/2} - 1\right\}\right) \qquad (9)$$

where Φ is the cone angle describing the amplitude of restricted motion. Calculated values of Φ are given in Table 6. The indole moiety of Trp59 shows an increase in the cone angle of as much as 5° in the circularly permuted variants compared to wild-type RNase T1. Average rotational differences reflected in steady-state polarization values (Table 6) correlate well with variations in the reported cone angles.

Iodide and Acrylamide Quenching. The single lifetime of Trp59 in the folded form of each of the RNase T1 proteins was measured at 10 °C and pH 5.0 as a function of both iodide and acrylamide concentration to assess the accessibility of this internal probe to quenching. Decreases in the apparent lifetime were analyzed according to eq 2 to give

Table 6: Trp59 Rotational Characteristics in RNase T1 Variants Denatured in 6 M GdmCl at 10 °C, pH 5.0[a]

		non-associative model[b]			associative model[c]			
protein	pol	$(r_0 - r_\infty)$	$\phi 1$ (ns)	Φ (deg)	$(r_0 - r_\infty)_{-l}$	$\phi 1_{-l}$ (ns)	$(r_0 - r_\infty)_{-s}$	$\phi 1_{-s}$ (ns)
wt	0.179 ± 0.002	0.122 ± 0.004	0.953 ± 0.066	36.0 ± 1.1	0.24 ± 0.41	1.13 ± 1.01	0.30 ± 0.31	0.075 ± 0.29
C2,10A	0.176 ± 0.002	0.127 ± 0.004	0.937 ± 0.066	36.5 ± 0.9	0.21 ± 0.29	1.18 ± 0.61	0.32 ± 0.39	0.074 ± 0.35
cp35	0.173 ± 0.002	0.140 ± 0.004	1.05 ± 0.06	39.1 ± 0.8	0.22 ± 0.29	1.25 ± 0.61	0.27 ± 0.36	0.087 ± 0.30
cp49	0.162 ± 0.002	0.153 ± 0.005	0.993 ± 0.058	41.5 ± 0.8	0.24 ± 0.28	1.24 ± 0.61	0.37 ± 0.35	0.060 ± 0.34
cp70	0.159 ± 0.002	0.149 ± 0.003	0.829 ± 0.047	40.8 ± 0.7	0.24 ± 0.32	1.29 ± 0.61	0.28 ± 0.29	0.085 ± 0.25
cp96	0.171 ± 0.002	0.137 ± 0.004	1.00 ± 0.061	38.5 ± 0.8	0.22 ± 0.30	1.26 ± 0.63	0.25 ± 0.34	0.059 ± 0.29

[a] Symbols used in this table correspond to the following: pol, steady-state polarization; $(r_0 - r_\infty)$, pre-exponential amplitude for fast rotation; $\phi 1$, rotational correlation time for fast rotation; subscripts "-l" and "-s" are used to denote the long- and short-lifetime components, respectively. [b] A non-associative model involves linking both lifetime components to a single set of rotational parameters. The variables r_0 and $\phi 2$ were linked across all data sets, giving values of 0.27 ± 0.01 and 8.76 ± 0.33 ns, respectively. A global κ^2 for this fit is 1.39. [c] An associative model allows each lifetime component to be described by its own unique set of rotational parameters. The variables r_0 and $\phi 2$ were linked across all data sets, giving values of 0.37 ± 0.03 and 9.45 ± 0.21 ns, respectively. A global κ^2 for this fit is 1.08.

values for the bimolecular rate constant k_{SV} (Table 4), describing the collision between quenching molecule and the excited state of the tryptophan. Results indicate almost no exposure of the indole moiety in the RNase T1 molecules to iodide ($k_{SV} < 0.02$ M^{-1} ns^{-1}), while acrylamide has only slight accessibility ($k_{SV} \leq 0.1$ M^{-1} ns^{-1}). NATA under identical conditions exhibits k_{SV} values of 3.20 ± 0.07 M^{-1} ns^{-1} and 4.17 ± 0.09 M^{-1} ns^{-1} for iodide and acrylamide, respectively. Clearly, the intrinsic tryptophan remains buried in the protein matrix in all of the mutants, as has previously been published for wild-type RNase T1 (Eftink & Ghiron, 1976, 1977; Eftink, 1983; Lakowicz *et al.*, 1983; James *et al.*, 1985).

The two lifetimes exhibited by Trp59 within the proteins denatured in 6M gdmCl have quite contrasting accessibilities to quencher (Table 3). For both iodide ions and acrylamide, the short-lifetime component ($\tau 1$) is quenched with a k_{SV} approximately 2−3-fold that of the long-lifetime component ($\tau 2$). A comparison between the RNase T1 proteins indicates that $\tau 1$ and $\tau 2$ generally have associated k_{SV} values larger for the circular permuted variants than for wild-type and C2,-10A. In particular, the tryptophan of unfolded cp49 is most exposed to collision with charged and uncharged molecules.

DISCUSSION

Multiphasic Fluorescence Recovery Implicates Proline Isomerization in Slow Folding Steps of RNase T1 Mutants. The unfolding transition, at least from the perspective of Trp59, in all cases can be described by a simple exponential decay, and the rate of unfolding changes uniformly with denaturant concentration (Figure 2). These data are consistent with an unfolding equilibrium between only two discrete states of the protein. The fluorescence recovery concomitant to folding, in contrast, is characterized by three distinct phases for all six proteins: a "fast" phase complete in a matter of a few seconds; an "intermediate" phase on the order of hundreds of seconds; and a "very slow" phase occurring over thousands of seconds. The complex nature of folding can be attributed to a conformationally heterogeneous population in the unfolded state. In native RNase T1, Schmid's laboratory has attributed this heterogeneity to a mixture of proline isomers around Pro39 and Pro55 (Scheme 1). The high similarity of the nature of fluorescence recovery between RNase T1, C2,10A, and each of the circularly permuted variants suggests that proline isomerizations still represent the rate-limiting steps during folding. However, there are real differences in the corresponding relative amplitudes and rate constants between the proteins (Table 2). The relative amplitude of the "fast" phase of fluorescence recovery is nearly 40% for native RNase T1, but it drops to near 20% for C2,10A, cp35, and cp96 and below 15% for cp49 and cp70. This "fast" phase represents rapidly formed intermediates with native-like secondary structure as well as a small percentage of molecules already containing Pro39 and Pro55 in the proper configuration (*cis*). Since the percentages of native molecules extrapolated to zero folding time are 3%−4% for all of the proteins examined, the decrease of the "fast" phase amplitude in fluorescence recovery must derive from differences in the contribution from intermediate species between the proteins. It is likely that the folding intermediates of each protein have differentially been destabilized and, therefore, either become contributors to the "intermediate" phase of folding or simply no longer can assume a tertiary fold with native-like fluorescence properties. Indeed, increasing the destabilizing conditions of folding by adding denaturant to the assay buffer systematically depletes the "fast" phase of folding (Table 2).

While the relaxation times of the "intermediate" phase are nearly identical between all but cp49, that of the "very slow" phase varies substantially from 5000 s in wild-type RNase T1 to 1300 s in cp49. These differences strongly correlate with the relative stabilities (Table 1) of the proteins, *i.e.*, the less stable the variant the faster the fluorescence recovery rate of its "very slow" phase. The increased rates of the "very slow" phase with progressively decreased stability in the RNase T1 variants could therefore result either from global instabilities of the intermediate(s) populating the folding pathway and/or from the release of a specific tertiary contact within the rapidly formed secondary structure of the intermediate(s). The intermediates do have variable stabilities between the mutants that relate somewhat with the trends in $[gdmCl]_{1/2}$ (Table 1), as seen by the different denaturant concentrations required to unfold each in the final assay step for intermediate formation. Also consistent with this idea, the "very slow" phase of fluorescence recovery in the four most stable proteins (WT, C2,10A, cp35, and cp96) is accelerated when denaturant concentrations are elevated and, presumably, destabilize the respective intermediate (Table 2).

Kinetics of Intermediate and Native Molecule Formation Reveal Differences in Rate but Not Mechanism in Slow Folding between RNase T1 Variants. On the basis of Scheme 1, the kinetic folding rate constants obtained for

wild-type RNase T1 are very similar to those reported previously (Kiefhaber *et al.*, 1990b). Relaxation times for native RNase T1 at 10 °C, pH 5.0, have been reported as 170, 6500, 400, and 250 s for τ_1, τ_3, τ_5, and τ_7, respectively (Kiefhaber *et al.*, 1990b). In this investigation, values for relaxation times of τ_1, τ_5, and τ_7 all range from approximately 150 to 350 s and therefore cumulatively comprise much of the "intermediate" phase in fluorescence recovery experiments (Table 3). The rate constant k_3 is the smallest by an order of magnitude, having a corresponding relaxation time of 7500 s. It has been previously suggested that a specific interaction between Trp59 and Pro39 in native RNase T1 interferes with the *trans*→*cis* isomerization of Pro39 in the $I_{55c}^{39t} \rightarrow N_{55c}^{39c}$ step of Scheme 1, essentially trapping the intermediate and giving rise to this very long relaxation time (Kiefhaber *et al.*, 1992). Indeed, replacement of Trp59 by a less bulky tyrosine did not affect stability but did increase the rate constant k_3 over 6-fold (Kiefhaber *et al.*, 1992).

The mutant C2,10A, lacking the short stabilizing disulfide bond, exhibits similar values for k_1, k_3, and k_5, but an almost 5-fold decrease in k_7, the rate constant for the isomerization of proline 55 to yield native molecules. Apparently, the absence of the short Cys2-Cys10 disulfide bond and/or the placement of alanines in these positions somehow perturbs the tertiary fold specifically of the intermediate I_{55t}^{39c} so as to disrupt subsequent configurational rearrangements around the Ser54-Pro55 bond, similar in nature but not magnitude to the constraints imposed upon I_{55c}^{39t}. The four circularly permuted mutants, for which C2,10A is essentially a positive control accounting for folding differences imparted by the Cys→Ala mutations, exhibit k_7 values similarly diminished relative to that of wild-type RNase T1. While corresponding relaxation times are somewhat varied for k_1 and k_5 describing the four transposed mutants, there are no systematic differences and values remain roughly between 100 and 300 s. However, calculated values of k_3, like the "very slow" phase rate constants for fluorescence recovery, are significantly increased relative to that of wild-type RNase T1 and C2,-10A and again correlate somewhat with the relative stabilities of the circularly permuted variants.

Dynamics of Trp59 Are Unaltered by Sequence Transpositions in Folded RNase T1 but Vary in the Denatured State. Not only does the intrinsic tryptophan provide an ideal probe to monitor the unfolding and folding of RNase T1, but the tryptophan itself is also instrumental in defining the folding characteristics of the protein. Trp59 has been implicated (Kiefhaber *et al.*, 1992) in impairing the isomerization of Pro39 in the I_{55c}^{39t} species of native RNase T1, which gives rise to the slowest step in the branched folding pathway. Since it is this slow step which is conspicuously increased to varying degrees by the sequence transpositions, it is possible that changes in the structural orientation and/or dynamics of Trp59 largely define differences in the slow folding between the RNase T1 mutants. To pursue this possibility, Trp59 in each of the six proteins was characterized at 10 °C, pH 5.0, in terms of its lifetime, accessibility to quenching, and rotational properties. Both "endpoints" of the folding process were examined, *i.e.*, fully folded and fully denatured forms of the proteins were investigated.

When fully folded, Trp59 in all of the six proteins exhibits essentially the same single exponential lifetime, approximately 3.8−4.2 ns (Table 4). Quenching of this lifetime by either iodide ions or acrylamide is very limited (Table 4), suggesting that the circular permutations, even those in which new termini were introduced near the tryptophan in primary sequence (cp49 and cp70), do not disrupt the protective hydrophobic core around the probe. Indeed, in every case, Trp59 remains so buried that only a single mode of rotation corresponding to diffusion of the entire protein is detected by dynamic anisotropy measurements (Table 4). This is consistent with previous fluorescence studies on wild-type RNase T1 (Lakowicz *et al.*, 1983; Eftink, 1983; James *et al.*, 1985; Axelson & Prendergast, 1989) and with crystal structure computations which found that unoccupied space around Trp59 allows the side chain to rotate no more than an undetectable ±5° (Axelson & Prendergast, 1989).

Complexities predictably arise when examining the fluorescence properties of each of the "fully" denatured RNase T1 proteins. The fluorescence lifetime, for example, cannot be modeled as a simple exponential but fits best to the sum of two discrete exponential decays (4.2−4.5 and 1.3−1.8 ns), each of which has distinctly different characteristics. The larger of the two lifetime components is approximately 3 times less accessible to acrylamide quenching and 2−3 times less accessible to quenching by iodide ions than the short-lifetime component (Table 5). Collisional rate constants for the short-lifetime component are slightly less but similar to those of NATA, a molecule that simulates a tryptophan free in solution flanked by peptide bonds. Moreover, when the rotational properties of the two lifetime components are analyzed separately, the amplitude and, to a greater extent, the rate of local motion are larger for the short-lifetime component (Table 6). These data suggest that at least two *distinct* microenvironments exist for the indole moiety of Trp59 within all six proteins under solution conditions (6 M gdmCl, pH 5.0) in which each was presumed to be completely unfolded. It is still not clear what, if any, residual structure might exist under denaturing conditions to continue to give rise to the two uniquely defined lifetime components. There is precedence in the literature on the basis of NMR studies that protein structure may persist in the unfolded states of proteins due to hydrophobic clustering (Evans *et al.*, 1991). Certainly the region encompassing Trp59 in RNase T1 could be susceptible to such phenomena. Pace *et al.* (1990) have shown that the average fractional change in the degree of exposure of groups when RNase T1 unfolds ($\Delta\alpha$) is markedly less than that of barnase, a related protein with a very similar folded conformation (Hill *et al.*, 1983). More specifically, Pace *et al.* (1992) have demonstrated through solvent perturbation difference spectroscopy that the tyrosine and tryptophan residues of reduced RNase T1 are significantly less accessible to perturbation by dimethyl sulfoxide in 8 M urea, pH 6.0, than are those of barnase.

The dynamics of Trp59 within the unfolded proteins can be more easily compared between the proteins by taking the simplified approach of designating a single set of rotational parameters to both lifetimes. When this is done, it becomes clear that, while there are no significant differences in the rate of local motion of the indole moiety between RNase T1 and the circularly permuted variants, the amplitude of local motion varies and correlates quite well with differences in steady-state polarization, variations in exposure to iodide and acrylamide quenching, and, most importantly, with relative folding rates of the slowest isomerization step. In the unfolded state, those proteins which reisomerize the

fastest in the $I_{55c}^{39t} \rightarrow N_{55c}^{39c}$ step also exhibit the greatest flexibility around the tryptophan side chain. It is possible that a looser protein matrix around Trp59 could preclude rigid interactions capable of trapping I_{55c}^{39t}. Of course, the dynamic characteristics of Trp59 within the intermediate itself are most relevant to potential steric restraints imposed on proline 39 isomerization. It is reasonable that differences evident in the unfolded state, itself shown to exhibit some form of structure, might also be manifested within the *partially* folded transients, despite the near identity of Trp59 characteristics in the fully folded proteins.

ACKNOWLEDGMENT

We are grateful to James B. Garrett for the initial construction and sequence verification of the genes for each of the circularly permuted variants. We also thank Arthur E. Johnson of the Department of Medical Biochemistry at Texas A&M University for extensive use of the model 8100 SLM steady-state fluorimeter and Gregory D. Reinhart of the Department of Biochemistry and Biophysics at Texas A&M University for use of the ISS K2 frequency−domain fluorimeter. We thank C. Nick Pace for his critical reading of the manuscript and continued support.

REFERENCES

Axelson, P. H., & Prendergast, F. G. (1989) *Biophys. J. 56*, 43−66.
Buchwalder, A., Szadkowski, H., & Kirschner, K. (1992) *Biochemistry 31*, 1621−1630.
Chen, L. X.-Q., Longworth, J. W., & Fleming, G. R. (1987) *Biophys. J. 51*, 865−873.
Eftink, M. R. (1983) *Biophys. J. 43*, 323.
Eftink, M. R., & Ghiron, C. A. (1976) *Biochemistry 15*, 672.
Eftink, M. R., & Ghiron, C. A. (1977) *Biochemistry 16*, 5546.
Eftink, M. R., & Ghiron, C. A. (1987) *Biophys. J. 52*, 467−473.
Evans, P. A., Topping, K. D., Woolfson, D. N., & Dobson, C. M. (1991) *Proteins: Struct., Funct., Genet. 9*, 248.
Garrett, J. B., Mullins, L. S., & Raushel, F. M. (1996) *Protein Sci. 5*, 204−211.
Goldenberg, D. P. (1989) *Protein Eng. 2*, 493−495.
Goldenberg, D. P., & Creighton, T. E. (1984) *J. Mol. Biol. 179*, 527−545.
Grathwohl, C., & Wuthrich, K. (1976) *Biopolymers 15*, 2025−2041.
Gratton, E. R., Alcala, J. R., & Marriott, G. (1986) *Biochem. Soc. Trans. 14*, 835−838.
Gryczynski, I., Eftink, M., & Lakowicz, J. R. (1988) *Biochim. Biophys. Acta 954*, 244−252.
Hill, C., Dodson, G., Heinemann, U., Saenger, W., Mitsui, Y., Nakamura, K., Borisov, S., Tischenko, G., Polyakov, K., & Pavlovsky, S. (1983) *Trends Biochem. Sci. 8*, 364.
Hu, C. Q., Sturtevant, J. M., Erickson, R. E., & Pace, C. N. (1992) *Biochemistry 31*, 4876−4882.
James, D. R., Demmer, D. R., Steer, R. P., & Verrall, R. E. (1985) *Biochemistry 24*, 5517−5526.
Jameson, D. M., Gratton, E., & Hall, R. D. (1984) *Appl. Spectrosc. Rev. 20*, 55−106.
Johnson, J. L., & Reinhart, G. D. (1994) *Biochemistry 31*, 11510−11518.
Kiefhaber, T., Quaas, R., Hahn, U., & Schmid, F. X. (1990a) *Biochemistry 29*, 3053−3061.
Kiefhaber, T., Quaas, R., Hahn, U., & Schmid, F. X. (1990b) *Biochemistry 29*, 3061−3070.
Kiefhaber, T., Grunert, H.-P., Hahn, U., & Schmid, F. X. (1990c) *Biochemistry 29*, 6475−6480.
Kiefhaber, T., Grunert, H.-P., Hahn, U., & Schmid, F. X. (1992) *Proteins: Struct., Funct., Genet. 12*, 171−179.
Lakowicz, J. R., Maliwal, B. P., Cherek, H., & Balter, A. (1983) *Biochemistry 22*, 1741.
Lipari, G., & Szabo, A. (1980) *Biophys. J. 30*, 489−506.
Luger, K., Hommel, U., Herold, M., Hofsteenge, J., & Kirschner, K. (1989) *Science 243*, 206−2443.
Mayr, L. M., & Schmid, F. X. (1993) *J. Mol. Biol. 231*, 913−926.
Mayr, L. M., Landt, O., Hahn, U., & Schmid, F. (1993) *J. Mol. Biol. 231*, 897−912.
Mullins, L. S., Wesseling, K., Kuo, J. M, Garret J. B., & Raushel, F. M. (1994) *J. Am. Chem. Soc. 32*, 6152−6156.
Munro, I., Pecht, I., & Stryer, L. (1979) *Proc. Natl. Acad. Sci. U.S.A. 76*, 56−60.
Oshima, T., Uenishi N., & Imahori, K. (1976) *Anal. Biochem. 71*, 632−634.
Pace, C. N. (1986) *Methods Enzymol. 131*, 266−279.
Pace, C. N., Laurents, D. V., & Thomson, J. A. (1990) *Biochemistry 29*, 2564−2572.
Pace, C. N., Laurents, D. V., & Erickson, R. E. (1992) *Biochemistry 31*, 2728−2734.
Perrin, F. (1926) *J. Phys. Radium 7*, 390−398.
Santoro, M. M., & Bolen, D. W. (1988) *Biochemistry 27*, 8063−8068.
Shirley, B., & Laurents, D. (1990) *J. Biochem. Biophys. Methods 20*, 181−188.
Spencer, R. D., & Weber, G. (1970) *J. Chem. Phys. 52*, 1654−1663.
Steyaert, J., Hallenga, K., Wyns, L., & Stanssens, P. (1990) *Biochemistry 29*, 9064−9072.
Tanford, C. (1968) *Adv. Protein Chem. 23*, 121−282.
Tartof, K. D., & Hobb, C. A. (1987) *Bethesda Res. Lab. Focus 9*, 12.
Viguera, A. R., Blanco, F. J., & Serrano, L. (1995) *J. Mol. Biol. 247*, 670−681.
Weber, G. (1952) Biochemistry *51*, 145−155.
Yang, Y. R., & Schachman, H. K. (1993) *Proc. Natl. Acad. Sci. U.S.A. 90*, 11980−11984.
Zell, R., & Fritz, H. J. (1987) *EMBO J. 6*, 1809−1815.
Zhang, T., Bertelson, E., Benvegnv, D., & Alber, T. (1993) *Biochem. 32*, 12311−12318.

BI953026P